7052 *Inorg. Chem.* **2010**, *49*, 7052–7056
DOI: 10.1021/ic1007236

Inorganic Chemistry
Article

A Heteroleptic Bis(tridentate)ruthenium(II) Polypyridine Complex with Improved Photophysical Properties and Integrated Functionalizability

Aaron Breivogel, Christoph Förster, and Katja Heinze*

Institute of Inorganic Chemistry and Analytical Chemistry, Johannes Gutenberg-University of Mainz,
Duesbergweg 10−14, 55128 Mainz, Germany

Received April 15, 2010

The synthesis and photophysical properties of a ruthenium(II) complex bearing an electron-accepting 2,2′;6′,2″-terpyridine ligand and an electron-donating *N*,*N*′-dimethyl-*N*,*N*′-dipyridin-2-ylpyridine-2,6-diamine (ddpd) ligand are presented. The heteroleptic complex is easily prepared isomerically pure and features intense low-energy metal-to-ligand charge-transfer (MLCT) absorption bands and intense room temperature ^{3}MLCT emission with a long ^{3}MLCT lifetime. The favorable photophysical properties are due to the strong ligand field imposed by the ddpd ligand.

Introduction

Meridional-coordinating tridentate ligands are preferred over bidentate ligands because of increased (photo)stability, absence of chirality (Δ and Λ), and simple functionalization in central mutually trans positions. For example, switching from tris(bidentate) $[\mathrm{Ir(ppy)_2(bpy)}]^+$ to bis(tridentate) $[\mathrm{Ir(phbpy)_2}]^+$ has been beneficial in terms of the stability and excited-state lifetime (ppy = 2-phenylpyridine; bpy = 2,2′-bipyridine; phbpy = 6-phenyl-2,2′-bipyridine).[1] However, in ruthenium oligopyridine chemistry, $[\mathrm{Ru(tpy)_2}]^{2+}$ (**1**) shows disappointing photophysical properties [essentially nonluminescent at room temperature and a low triplet-state metal-to-ligand charge-transfer (^{3}MLCT) lifetime] compared to $[\mathrm{Ru(bpy)_3}]^{2+}$ (**2**). Thermal population of a low-lying ^{3}MC state of **1** provides an efficient deactivating pathway.[2−4]

Two strategies have emerged to improve the excited-state properties of bis(tridentate) ruthenium complexes: (i) increasing the M−L orbital overlap by adjusting the bite angles from N−Ru−N < 80° in five-membered chelate rings to ~90° in six-membered chelate rings, which raises the energy of the ^{3}MC state relative to that of the ^{3}MLCT state,[5−10] and (ii) attaching an electron-withdrawing substituent to lower the oligopyridine π^* orbitals and thus the energy of the MLCT states relative to the deactivating ^{3}MC state (which should overcompensate for the effect of increased nonradiative decay at low emission energies).[11−14] Concomitant attachment of an electron-donating substituent at the second chelate ligand further improves the emission properties.[14,15] These effects are clearly seen in the series $[\mathrm{Ru(tpy)_2}]^{2+}$ (**1**; $\lambda_{\mathrm{abs/emiss}}$ = 474/629 nm[11]) → $[\mathrm{Ru(EtOOC\text{-}tpy)(tpy)}]^{2+}$ (**3**; 485/667 nm[13]) → $[\mathrm{Ru(EtOOC\text{-}tpy)(H_2N\text{-}tpy)}]^{2+}$ (**4**; 500/744 nm[14,15]) (Chart 1). At room temperature, the luminescence quantum yield increases from $< 5 \times 10^{-6}$ to 2.7×10^{-4} to 1.8×10^{-3} and the excited-state lifetime from 0.25 to 32 to 34 ns.[11,13−15] Hammarström et al. have switched five-membered chelate rings to six-membered chelate rings by employing (bipyridylpyridyl)methane derivatives (bpy-$\mathrm{CR_2}$-py) instead of terpyridine.[5] The homoleptic

---

*To whom correspondence should be addressed. E-mail: katja.heinze@uni-mainz.de. Fax: +49-6131-39-27277.

(1) Tinker, L. L.; Bernhard, S. *Inorg. Chem.* **2009**, *48*, 10507.

(2) Sauvage, J.-P.; Collin, J.-P.; Chambron, J.-C.; Guillerez, S.; Coudret, C.; Balzani, V.; Barigelletti, F.; De Cola, L.; Flamigni, L. *Chem. Rev.* **1994**, *94*, 993.

(3) Winkler, J. R.; Netzel, T. L.; Creutz, C.; Sutin, N. *J. Am. Chem. Soc.* **1987**, *109*, 2381.

(4) Siemeling, U.; Vor der Brüggen, J.; Vorfeld, U.; Neumann, B.; Stammler, A.; Stammler, H.-G.; Brockhinke, A.; Plessow, R.; Zanello, P.; Laschi, F.; Fabrizi de Biani, F.; Fontani, M.; Steenken, S.; Stapper, M.; Gurzadyan, G. *Chem.—Eur. J.* **2003**, *9*, 2819.

(5) Abrahamsson, M.; Wolpher, H.; Johansson, O.; Larsson, J.; Kritikos, M.; Eriksson, L.; Norrby, P.-O.; Bergquist, J.; Sun, L.; Åkermark, B.; Hammarström, L. *Inorg. Chem.* **2005**, *44*, 3215.

(6) Abrahamsson, M.; Jäger, M.; Österman, T.; Eriksson, L.; Persson, P.; Becker, H.-C.; Johansson, O.; Hammarström, L. *J. Am. Chem. Soc.* **2006**, *128*, 12616.

(7) Abrahamsson, M.; Jäger, M.; Kumar, R. J.; Österman, T.; Persson, P.; Becker, H.-C.; Johansson, O.; Hammarström, L. *J. Am. Chem. Soc.* **2008**, *130*, 15533.

(8) Jäger, M.; Kumar, R. J.; Görls, H.; Bergquist, J.; Johansson, O. *Inorg. Chem.* **2009**, *48*, 3228.

(9) Kumar, R. J.; Karlsson, S.; Streich, D.; Rolandini Jensen, A.; Jäger, M.; Becker, H.-C.; Bergquist, J.; Johansson, O.; Hammarström, L. *Chem.—Eur. J.* **2010**, *16*, 2830.

(10) Jäger, M.; Smeigh, A.; Lombeck, F.; Görls, H.; Collin, J.-P.; Sauvage, J.-P.; Hammarström, L.; Johansson, O. *Inorg. Chem.* **2010**, *49*, 374.

(11) Maestri, M.; Armaroli, N.; Balzani, V.; Constable, E. C.; Cargill Thompson, A. M. W. *Inorg. Chem.* **1995**, *34*, 2759.

(12) Schubert, U. S.; Hofmeier, H.; Newkome, G. R. *Modern Terpyridine Chemistry*; Wiley-VCH: Weinheim, Germany, 2006.

(13) Bolink, H. J.; Cappelli, L.; Coronado, E.; Gaviña, P. *Inorg. Chem.* **2005**, *44*, 5966.

(14) Heinze, K.; Hempel, K.; Beckmann, M. *Eur. J. Inorg. Chem.* **2006**, 2040.

(15) Heinze, K.; Hempel, K.; Tschierlei, S.; Schmitt, M.; Popp, J.; Rau, S. *Eur. J. Inorg. Chem.* **2009**, 3119.

Chart 1. Bis(tridentate) Ruthenium(II) Oligopyridine Complexes

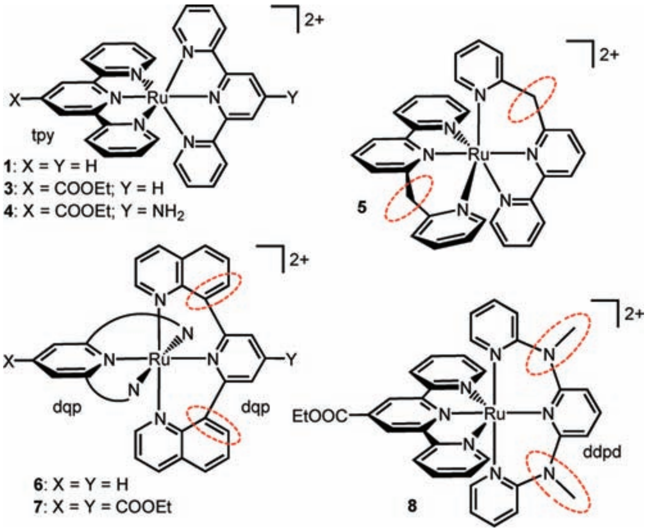

bis[(bipyridylpyridyl)methane]ruthenium complex **5** features τ = 15 ns and $\Phi = 10^{-3}$ ($\lambda_{\mathrm{abs/emiss}}$ = 477/655 nm; Chart 1).[5] However, the values are still well below those of the tris-bpy complex **2** (τ = 1 μs, $\Phi = 8.9 \times 10^{-2}$[6,7]), and **5** is still chiral. These properties have been surpassed by the homoleptic complex $[\mathrm{Ru(dqp)_2}]^{2+}$ (**6**, Chart 1). Almost 90° N−Ru−N bite angles are observed and excellent photophysical properties are achieved ($\Phi = 2 \times 10^{-2}$; τ = 3 μs; $\lambda_{\mathrm{abs/emiss}}$ = 490/700 nm). Further enhancement is achieved by COOEt substitution (**7**, Chart 1; $\Phi = 7 \times 10^{-2}$; τ = 5.5 μs; $\lambda_{\mathrm{abs/emiss}}$ = 553/693 nm).[6,7]

However, these homoleptic dqp complexes show *fac*/*mer* stereoisomerism because of the flexible six-membered chelate rings (the *fac* isomers even come in cis-*fac* and trans-*fac* isomers), and, in addition, $\mathrm{N_5Cl}$-coordinated complexes $[\mathrm{RuCl(dqp)_2}]^{+}$ are formed.[8] Heteroleptic-type **6** complexes with X ≠ Y (e.g., donor/acceptor substitution) are quite difficult to obtain,[8] but very recently Hammarström et al. succeeded in incorporating dqp complexes in donor/chromophor/acceptor triads.[9]

Results and Discussion

Here we describe the synthesis and properties of the heteroleptic ruthenium oligopyridine complex **8** (Chart 1), which has several beneficial features: a 2-fold rotation axis, setup for simple functionalization in the direction of this C_2 axis,[16] absence of *fac*/*mer* stereoisomerism, an electron-donating *N*,*N*′-dimethyl-*N*,*N*′-dipyridin-2-ylpyridine-2,6-diamine (ddpd) ligand forming six-membered chelate rings together with an electron-withdrawing 4′-(ethylcarboxy)terpyridine ligand (push−pull substitution). The methyl substituents of ddpd are necessary because tripyridyldiamines lacking alkyl groups at the amine are easily deprotonated, yielding chain complexes that are interesting by themselves for other reasons but undesirable for our purposes.[17]

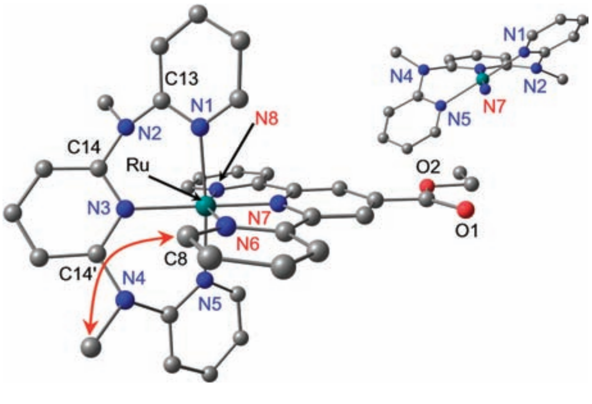

Figure 1. DFT (B3LYP, LANL2DZ)-optimized geometry of **8** (inset: Newman projection viewed approximately along the C_2 axis; tpy-COOEt ligand omitted). Hydrogen atoms are omitted for clarity. The arrow indicates an interligand NOE contact between protons.

First, we performed quantum chemical calculations on the homoleptic complex $[\mathrm{Ru(ddpd)_2}]^{2+}$ (**9**). The calculations suggest that *fac*/*mer* stereoisomers are analogous to those of **6**, with *mer*-**9** being more stable than *trans*-*fac*-**9** (31 kJ mol^{-1}) and *cis*-*fac*-**9** (34 kJ mol^{-1}). Attempts to synthesize and purify **9** are indeed complicated because of the formation of *fac*/*mer* isomers and $\mathrm{N_5Cl}$ coordination. Coordinated chloride is easily removed by silver cations, but heating (dimethyl sulfoxide, reflux, microwave, 10 h) does not furnish pure *mer*-**9**. The photophysical properties of the *fac*/*mer* mixture were also disappointing ($\lambda_{\mathrm{abs/emiss}}$ = 393/468 nm, very weak emission). Thus, we switched to the mixed donor/acceptor-substituted ruthenium(II) complex **8** with an electron-donating ddpd ligand and an electron-withdrawing EtOOC-tpy ligand. **8** is easily prepared from $\mathrm{RuCl_3(EtOOC\text{-}tpy)}$[18−20] and ddpd in a microwave-assisted synthesis at 80 °C (after chloride abstraction with silver nitrate and precipitation with $\mathrm{NH_4PF_6}$) as a purple powder in 62% yield.

High-resolution electrospray ionization [(HR)ESI] mass spectrometry (MS), IR spectrometry, multinuclear and correlation NMR spectroscopy, and elemental analysis are consistent with the formulated structure of **8**. Because the tpy ligand only coordinates in a meridional fashion, *fac*/*mer* stereoisomers are absent. A single resonance is observed for the $\mathrm{N-CH_3}$ hydrogen, carbon, and nitrogen nuclei, respectively (Supporting Information). Singlet ground-state density functional theory (DFT) calculations on **8** reveal that the N−Ru−N angles involving the ddpd ligand are around 88° while the corresponding angles involving the tpy ligand are around 79° (Figure 1). The six-membered chelate rings of the ddpd ligand form boat conformations, resulting in an overall small twist of the ddpd ligand, with one terminal pyridine ring pointing up and the other one pointing down relative to the plane of the central pyridine ring (Figure 1, inset). Similarly, the $\mathrm{N-CH_3}$ groups point up and below the central pyridine plane ($\mathrm{H_3\underline{C}-\underline{N}2-\underline{C}14-\underline{N}3/H_3\underline{C}-\underline{N}4-\underline{C}14'-\underline{N}3}$ = 150.4°/150.2°), which allows for an nuclear Overhauser enhancement (NOE) contact to the tpy proton H8 vis-à-vis (indicated by an orange-colored arrow, Figure 1). Gratifyingly, the DFT-calculated metrical parameters match those obtained from a single-crystal X-ray diffraction analysis of **8** [triclinic, $P\bar{1}$; N1−Ru−N3/N5−Ru−N3 = 87.5°/87.7°; N6−Ru−N7/N7−Ru−N8 = 79.6°/79.7°; $\mathrm{H_3\underline{C}-\underline{N}2-\underline{C}14-\underline{N}3/H_3\underline{C}-\underline{N}4-\underline{C}14'-\underline{N}3}$ = 156.2°/153.2°; the atom numbering refers to that used in Figure 1 for the sake of comparison].

---

(16) Heinze, K.; Hempel, K. *Chem.—Eur. J.* **2009**, *15*, 1346.

(17) Yin, C.; Huang, G.-C.; Kuo, C.-K.; Fu, M.-D.; Lu, H.-C.; Ke, J.-H.; Shih, K.-N.; Huang, Y.-L.; Lee, G.-H.; Yeh, C.-Y.; Chen, C.-h.; Peng, S.-M. *J. Am. Chem. Soc.* **2008**, *130*, 10090.

(18) Fallahpour, R.-A. *Synthesis* **2000**, *8*, 1138.

(19) Fallahpour, R.-A. *Eur. J. Inorg. Chem.* **1998**, 1205.

(20) Fallahpour, R.-A.; Neuburger, M.; Zehnder, M. *New J. Chem.* **1999**, *23*, 53.

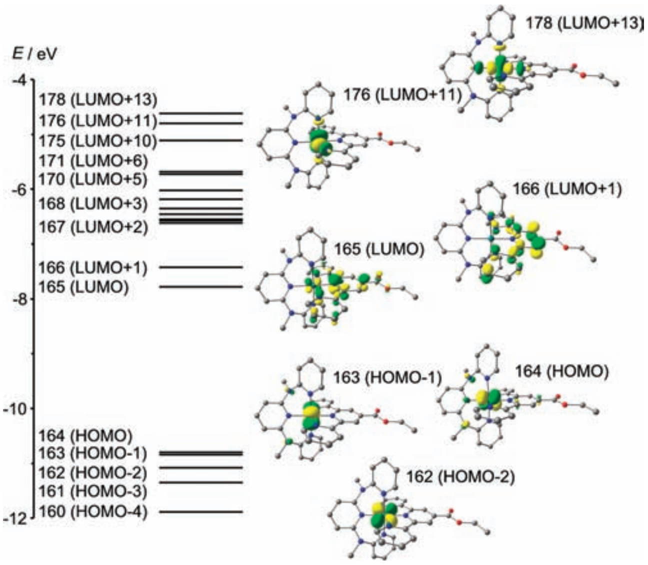

Figure 2. Molecular orbital diagram of **8** and some relevant molecular orbitals (contour value 0.06 au).

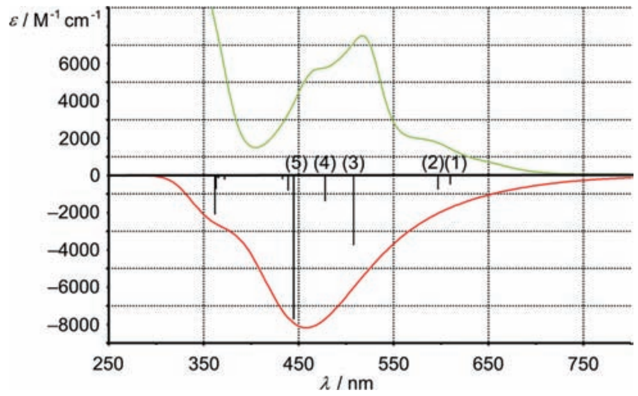

Figure 3. Experimental electronic absorption spectrum of **8** in CH_3CN (top) and calculated stick spectrum (TD-DFT, IEFPCM, CH_3CN) of **8** (the intensity of the sticks is proportional to the calculated oscillator strength, and the calculated spectrum is composed of δ functions at the excitation energies) (bottom).

Kohn−Sham frontier orbitals of the singlet ground state of **8** are shown in Figure 2. The lowest unoccupied molecular orbitals (LUMOs) of **8** are mainly localized on the EtOOC-tpy ligand, while the highest occupied molecular orbitals (HOMOs) are essentially ruthenium-based orbitals (t_{2g} in octahedral symmetry) with some ddpd contribution (especially the nitrogen atoms of the $N-CH_3$ groups). The experimental electronic spectrum of **8** is dominated by intense $\pi \rightarrow \pi^*$ transitions at $\lambda < 350$ nm (Supporting Information). The broad absorption band around $\lambda = 500$ nm corresponds to several MLCT transitions (Figure 3).[21] On the basis of time-dependent DFT (TD-DFT) calculations (gas-phase and polarizable continuum solvation model, CH_3CN)[21] on **8** involving the first 12 spin-allowed singlet excitations, the most intense peaks in the visible spectral region are assigned to MLCT "t_{2g}(Ru)" → π^*(tpy-COOEt) transitions, e.g., transitions (3), (4), and (5) involve mainly HOMO, HOMO−1, and HOMO−2 (d_{Ru}) to LUMO and LUMO+1 [π^*(tpy-COOEt)] transitions at 508, 478, and 445 nm (Figures 2 and 3).

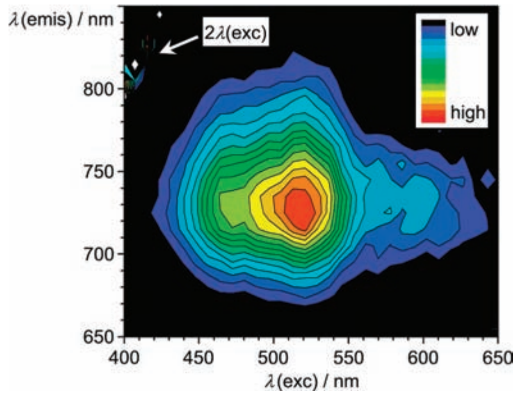

Figure 4. Excitation emission matrix of **8**.

The TD-DFT results compare well with the experimental data of **8** ($\lambda_{abs} = 517$ nm; $\varepsilon = 7500$ M^{-1} cm^{-1}; Figure 3). The difference between experimental and calculated absorption maxima of $\Delta E = 0.35$ eV (gas phase) [$\Delta E = 0.30$ eV (CH_3CN)] is similar to the one obtained for **1** using the same method [$\Delta E = 0.38$ eV (acetone)].[21] The experimental maximum of **8** is bathochromically shifted by 1275 cm^{-1} relative to that of **3** because of the π-electron-donating effect of ddpd, raising the energy of the Ru d orbitals.

The room temperature emission is also shifted from 667 nm (**3**) to 729 nm (**8**),[13] with the maximum intensity observed upon excitation of the ^{1}MLCT transitions (Figure 4). The excitation spectrum closely follows the absorption spectrum in the visible spectral region. In spite of the lower ^{3}MLCT energy, **8** features a more than 10-fold higher quantum yield compared to **3** [$\Phi = 3.0 \times 10^{-3}$ (**8**)]. Also, the ^{3}MLCT lifetime has dramatically increased to $\tau = 722(5)$ ns (**8**). This is appreciable considering the fact that a lower ^{3}MLCT energy should lead to faster nonradiative decay.[22,23]

In frozen butyronitrile at 77 K, emission is observed at higher energy and with a higher lifetime [$\lambda_{emiss} = 707$ nm; $\tau = 3309(15)$ ns]. The first observation is due to the lower stabilization of the excited state in the frozen matrix, and the second finding is due to less accessible thermal deactivation pathways. The DFT-calculated energy difference between the ^{3}MLCT state and the ground state (gas phase) amounts to 1.64 eV (756 nm for the $0 \rightarrow 0$ transition), in quite good agreement with the experiment.[21]

The photophysical properties of **8** are thus dramatically improved when compared to those of **1** and are approaching those of **2** ($\Phi = 6.2 \times 10^{-2}$; $\tau = 962$ ns[24,25]).

The $Ru^{II/III}$ oxidation of **8** is found at $E_{1/2} = 0.81$ V (vs Fc/Fc^+). Thus, **8** is harder to oxidize than **4** ($E_{1/2} = 0.68$ V[14]) but easier to oxidize than **1** ($E_{1/2} = 0.92$ V[11]) or **3** ($E_{1/2} = 0.96$ V[13]). This reflects the stronger donor ability of ddpd as compared to tpy, raising the energy of the Ru d levels. **8** is reduced at $E_{1/2} = -1.40$ V in a quasi-two-electron process, precluding assignments to individual ligands.

To place the ddpd ligand in the context of other donor ligands, a computational analysis was conducted. The net donor strength ($\sigma + \pi$) is estimated from DFT-calculated A_1 carbonyl stretching modes of tricarbonyl(nickel) fragments

---

(21) Jakubikova, E.; Chen, W.; Dattelbaum, D. M.; Rein, F. N.; Rocha, R. C.; Martin, R. L.; Batista, E. R. *Inorg. Chem.* **2009**, *48*, 10720.

(22) Meyer, T. J. *Pure Appl. Chem.* **1986**, *58*, 1193.

(23) Caspar, J. V.; Meyer, T. J. *J. Phys. Chem.* **1983**, *87*, 952.

(24) Caspar, J. V.; Meyer, T. J. *J. Am. Chem. Soc.* **1983**, *105*, 5583.

(25) Ding, Z.; Wellington, R. G.; Brevet, P. F.; Girault, H. H. *J. Phys. Chem.* **1996**, *100*, 10658.

coordinated to the ligands.[26,27] On this basis, the ddpd ligand was ranked between trimethylamine and N-heterocyclic carbene ligands (Supporting Information).

Conclusion

We have prepared a novel heteroleptic ruthenium(II) complex with a terpyridine acceptor ligand and a meridional-coordinating tridentate ddpd donator ligand. The latter forms six-membered chelate rings with the metal center. This ligand combination results in long-wavelength absorption and emission as well as an extended ^{3}MLCT lifetime of 722 ns.

The effects of ddpd are 3-fold: improved σ-orbital overlap with Ru "e_g" orbitals due to $\approx$90° bite angles (LUMO+11 and LUMO+13; Figure 2) raising their energies and thus the energy of the deactivating ^{3}MC state, increased σ-donation boosting this effect, and increased π donation raising the energy of the Ru "t_{2g}" orbitals and resulting in quite low absorption and emission energies. These aspects of ddpd will also be exploited in other ddpd metal complexes currently prepared in our group. The use of **8** and functionalized derivatives in organic light-emitting devices, dye-sensitized solar cells (DSSCs), or biolabeling applications is actively pursued in our group.

Experimental Section

General Procedures. CH_3CN and dioxane were distilled from CaH_2 and sodium, respectively. All reagents were used as received from commercial suppliers (Acros and Sigma-Aldrich). Microwave heating was performed in a Discover Benchmate Plus (CEM Synthesis) single-mode microwave cavity, producing continuous irradiation at 2.455 GHz with 100 W (maximum power). Reaction mixtures were stirred with a magnetic stir bar during irradiation. The temperature and irradiation power were monitored during the course of the reaction. NMR spectra were recorded on a Bruker Avance DRX 400 spectrometer at 400.31 MHz (^{1}H), 100.66 MHz (${}^{13}C\{{}^1H\}$), and 40.56 MHz (^{15}N). All resonances are reported in ppm versus the solvent signal as an internal standard [CD_3CN (^{1}H, $\delta = 1.94$; ^{13}C, $\delta = 1.24$ ppm)] or versus external CH_3NO_2 (90% in $CDCl_3$; ^{15}N, $\delta = 0$ ppm). IR spectra were recorded with a BioRad Excalibur FTS 3100 spectrometer as KBr disks. Electrochemical experiments were carried out on a BioLogic SP-50 voltammetric analyzer using platinum wires as counter and working electrodes and 0.01 M Ag/$AgNO_3$ as the reference electrode. The measurements were carried out at a scan rate of 150 mV s^{-1} for cyclic voltammetry experiments and at 50−200 mV s^{-1} for square-wave voltammetry experiments using 0.1 M (nBu$_4$N)(PF$_6$) as the supporting electrolyte in CH_3CN. Potentials are referenced to the ferrocene/ferrocenium couple ($E_{1/2} = 85 \pm 5$ mV under the experimental conditions). UV/vis/near-IR spectra were recorded on a Varian Cary 5000 spectrometer using 1.0 cm cells (Hellma, Suprasil). Emission spectra were recorded on a Varian Cary Eclipse spectrometer. Quantum yields were determined by comparing the areas under the emission spectra on an energy scale/cm^{-1} recorded for optically matched solutions of the sample and the reference {([Ru(bpy)$_3$]$^{2+}$) = 0.062 in CH_3CN}.[24] For time-resolved photoluminescence measurements, a solution ($c = 4.5 \times 10^{-6}$ M in butyronitrile) was filled into a homemade cuvette (tin-plated copper with quartz windows; indium-sealed; 4 mm optical path length) inside a nitrogen-filled glovebox and the cuvette was sealed and transferred to a home-built cryostat. It was kept under a dynamic vacuum (typically 10^{-6} mbar) for low-temperature experiments. The sample was excited by the 517 nm output of an optical parametric oscillator (OPO; GWU Lasertechnik) itself pumped by the frequency-tripled (10 Hz) output of a pulsed Nd:YAG nanosecond laser (INDI Quanta Ray Spectra Physics). The luminescence of the sample was dispersed by a Shamrock SR-303i spectrograph with a 150 L/mm grating and detected by a gated intensified CCD detector (Andor IStar DH740 ICCD camera). The solution was illuminated with the laser beam from the detector side, and measurements were conducted at room temperature (295 K) and liquid-nitrogen temperature (77 K). Single exponentials were used to fit the experimental data. Field desorption (FD) MS spectra were recorded on a FD Finnigan MAT90 spectrometer. ESI MS spectra were recorded on a Micromass Q-TOF-Ultima spectrometer. Elemental analyses were performed by the microanalytical laboratory of the chemical institutes of the University of Mainz.

Crystal Structure Determination. Intensity data were collected with a Bruker AXS Smart1000 CCD diffractometer with an APEX II detector and an Oxford cooling system and corrected for absorption and other effects using Mo Kα radiation ($\lambda = 0.710\,73$ Å) at 173(2) K. The diffraction frames were integrated using the *SAINT* package, and most were corrected for absorption with *MULABS*.[28,29] The structures were solved by direct methods and refined by the full-matrix method based on F^2 using the *SHELXTL* software package.[30,31] All non-hydrogen atoms were refined anisotropically, while the positions of all hydrogen atoms were generated with appropriate geometric constraints and allowed to ride on their respective parent carbon atoms with fixed isotropic thermal parameters. The asymmetric unit of a crystal of **8** contains one molecule of an acetonitrile solvent and two [PF$_6$]$^-$ counterions, one of which is disordered over two positions (site occupancy 0.73:0.27). Crystallographic data (excluding structure factors) for the structure reported in this paper have been deposited with the Cambridge Crystallographic Data Centre as supplementary publication no. CCDC-773229. Copies of the data can be obtained free of charge upon application to CCDC, 12 Union Road, Cambridge CB2 1EZ, U.K. [fax (0.44) 1223-336-033; e-mail deposit@ccdc.cam.ac.uk].

DFT calculations were carried out with the *Gaussian03*/DFT[32] series of programs. The B3LYP formulation of DFT was used by employing the LANL2DZ basis set.[32] No symmetry constraints were imposed on the molecules. For solvent modeling, the integral-equation-formalism polarizable continuum model (IEFPCM) was employed.

---

(26) Tolman, C. A. *Chem. Rev.* **1977**, *77*, 313.

(27) Shi, Q.; Thatcher, R. J.; Slattery, J.; Sauari, P. S.; Whitwood, A. C.; McGowan, P. C.; Douthwaite, R. E. *Chem.—Eur. J.* **2009**, *15*, 11346.

(28) *SMART Data Collection and SAINT-Plus Data Processing Software for the SMART System*, various versions; Bruker Analytical X-ray Instruments, Inc.: Madison, WI, 2000.

(29) Blessing, B. *Acta Crystallogr.* **1995**, *A51*, 33.

(30) Sheldrick, G. M. *SHELXTL*, version 5.1; Bruker AXS: Madison, WI, 1998.

(31) Sheldrick, G. M. *SHELXL-97*; University of Göttingen: Göttingen, Germany, 1997.

(32) Frisch, M. J.; Trucks, G. W.; Schlegel, H. B.; Scuseria, G. E.; Robb, M. A.; Cheeseman, J. R.; Montgomery, J. A.; Vreven, T., Jr.; Kudin, K. N.; Burant, J. C.; Millam, J. M.; Iyengar, S. S.; Tomasi, J.; Barone, V.; Mennucci, B.; Cossi, M.; Scalmani, G.; Rega, N.; Petersson, G. A.; Nakatsuji, H.; Hada, M.; Ehara, M.; Toyota, K.; Fukuda, R.; Hasegawa, J.; Ishida, M.; Nakajima, T.; Honda, Y.; Kitao, O.; Nakai, H.; Klene, M.; Li, X.; Knox, J. E.; Hratchian, H. P.; Cross, J. B.; Adamo, C.; Jaramillo, J.; Gomperts, R.; Stratmann, R. E.; Yazyev, O.; Austin, A. J.; Cammi, R.; Pomelli, C.; Ochterski, J. W.; Ayala, P. Y.; Morokuma, K.; Voth, G. A.; Salvador, P.; Dannenberg, J. J.; Zakrzewski, V. G.; Dapprich, S.; Daniels, A. D.; Strain, M. C.; Farkas, O.; Malick, D. K.; Rabuck, A. D.; Raghavachari, K.; Foresman, J. B.; Ortiz, J. V.; Cui, Q.; Baboul, A. G.; Clifford, S.; Cioslowski, J.; Stefanov, B. B.; Liu, G.; Liashenko, A.; Piskorz, P.; Komaromi, I.; Martin, R. L.; Fox, D. J.; Keith, T.; Al-Laham, M. A.; Peng, C. Y.; Nanayakkara, A.; Challacombe, M.; Gill, P. M. W.; Johnson, B.; Chen, W.; Wong, M. W.; Gonzalez, C.; Pople, J. A. *Gaussian 03*, revision B.03; Gaussian, Inc.: Pittsburgh, PA, 2003.

Chart 2. Atom Numbering of ddpd for NMR Assignment

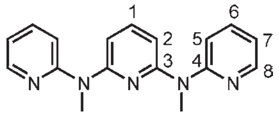

Chart 3. Atom Numbering of **8** for NMR Assignment

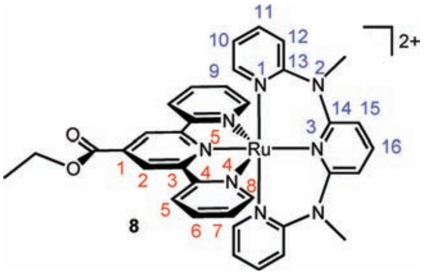

Synthesis of ddpd (Chart 2). Potassium bis(trimethylsilyl)-amide (5.670 g, 28.42 mmol, 2.6 equiv) was dissolved in dioxane (100 mL) under argon. After the addition of *N*-methylpyridin-2-ylamine (3.00 mL, 29.2 mmol, 2.7 equiv), the solution turned yellow. A solution of 2,6-dibromopyridine (2.555 g, 10.79 mmol, 1.0 equiv) in dioxane (30 mL) was added, and the mixture was heated to reflux for 64 h, resulting in a brown solution. After cooling to room temperature, water (250 mL) was added, and the aqueous phase was extracted three times with tetrahydrofuran/Et_2O (1:1, 100 mL). The combined organic phases were washed three times with a 1 M aqueous Na_2CO_3 solution and finally dried over $MgSO_4$. After removal of the solvent under reduced pressure, the product was purified by column chromatography (silica gel, 3:1 petroleum ether 40−60/ethyl acetate), yielding a yellow viscous liquid. Yield: 2.82 g (9.68 mmol, 90%). ^1H NMR (CD_3CN, 300 K): δ 8.29 (m, 2 H, H^8), 7.57 (m, 2 H, H^6), 7.50 (t, $^3J_{HH}$ = 8.0 Hz, 1 H, H^1), 7.26 (m, 2 H, H^5), 6.89 (m, 2 H, H^7), 6.71 (d, $^3J_{HH}$ = 8.0 Hz, 2 H, H^2), 3.50 (s, 6 H, CH_3). $^{13}C\{^1H\}$ NMR (CD_3CN, 300 K): δ 158.7 (s, C^4), 157.2 (s, C^3), 148.8 (s, C^8), 139.8 (s, C^1), 137.8 (s, C^6), 117.9 (s, C^7), 116.3 (s, C^5), 106.6 (s, C^2), 36.3 (s, CH_3). MS (FD): *m*/*z* 291.2 (100%) $[M]^+$. HR-MS (ESI^+): Calcd for $C_{17}H_{17}N_5Na$: *m*/*z* 314.1382. Obsd: *m*/*z* 314.1375. Elem anal. Calcd for $C_{17}H_{17}N_5$ (291.35): C, 70.08; H, 5.88; N, 24.04. Found: C, 70.12; H, 5.52; N, 24.34.

Synthesis of 8 (Chart 3). A solution of ddpd (216.4 mg, 0.743 mmol, 1.5 equiv) in ethanol (15 mL) was added to $RuCl_3$-(EtOOC-tpy)[33−35] (251.0 mg, 0.490 mmol, 1.0 equiv). After the addition of *N*-ethylmorpholine (0.20 mL, 0.18 mg, 3.2 equiv), the mixture was sonicated for 1 min and heated to reflux in a laboratory microwave oven for 15 min (80 °C). The mixture was filtered over Celite (1.5 cm; diameter 3.5 cm) and rinsed with ethanol. The solvent was removed under reduced pressure, and the dark-red-brown residue was dissolved in ethanol (3 mL). The addition of an aqueous solution of NH_4PF_6 (239.0 mg, 1.466 mmol, 3.0 equiv, 3 mL of H_2O) resulted in the precipitation of a purple solid. After the precipitate was washed with water, the precipitate was dissolved in CH_3CN (10 mL) and a solution of $AgNO_3$ (52 mg, 0.31 mmol, 0.4 equiv) in CH_3CN (10 mL) was added. The mixture was refluxed for 4 h. The resulting AgCl was removed by filtration, and the filtrate was concentrated to 3 mL under reduced pressure. The addition of an aqueous solution of NH_4PF_6 (156.0 mg, 0.957 mmol, 2.0 equiv, 3 mL of H_2O) resulted in the precipitation of a purple solid, which was collected by filtration and dried under reduced pressure. Yield: 298.6 mg (0.3023 mmol, 62%). Crystals suitable for single-crystal X-ray diffraction were obtained by the slow diffusion of diethyl ether into a solution of **8** in CH_3CN. ^1H NMR (CD_3CN, 300 K): δ 8.97 (s, 2 H, H^2), 8.56 (m, 2 H, H^5), 8.27 (t, $^3J_{HH}$ = 8.2 Hz, 1 H, H^{16}), 8.11 (m, 2 H, H^8), 8.02 (m, 2 H, H^6), 7.61 (m, 2 H, H^{11}), 7.56 (d, $^3J_{HH}$ = 8.2 Hz, 2 H, H^{15}), 7.47 (m, 2 H, H^7), 7.17 (m, 2 H, H^{12}), 6.57 (m, 2 H, H^{10}), 6.42 (m, 2 H, H^9), 4.58 (q, $^3J_{HH}$ = 7.1 Hz, 2 H, $C\underline{H}_2CH_3$), 3.46 (s, 6 H, $N{-}C\underline{H}_3$), 1.52 (t, $^3J_{HH}$ = 7.1 Hz, 3 H, $CH_2C\underline{H}_3$). $^{13}C\{^1H\}$ NMR (CD_3CN, 300 K): δ 164.9 (s, C═O), 159.8, 159.7 (2s, C^3, C^{13}), 158.7 (s, C^4), 157.2 (s, C^{14}), 155.1 (s, C^8), 149.4 (s, C^9), 141.8 (s, C^{16}), 140.2 (s, C^{11}), 139.2 (s, C^6), 136.3 (s, C^1), 128.0 (s, C^7), 125.7 (s, C^5), 123.8 (s, C^2), 121.5 (s, C^{10}), 116.3 (s, C^{12}), 113.6 (s, C^{15}), 63.7 (s, $\underline{C}H_2CH_3$), 41.8 (s, $N\underline{C}H_3$), 14.6 (s, $CH_2\underline{C}H_3$). $^1H{-}^{15}N$ HMBC (CD_3CN, 300 K): δ −288.1 (N^2), −168.6 (N^1), −162.2 (N^3), −142.2 (N^4), −85.8 (N^5). MS (ESI^+): *m*/*z* 349.1 (7%) $[M - 2PF_6]^{2+}$, 843.1 (100) $[M - PF_6]^+$. HR-MS (ESI^+): Calcd for $C_{35}H_{32}F_6N_8O_2P^{96}Ru$: *m*/*z* 837.1366. Obsd: *m*/*z* 837.1360. IR (KBr): $\tilde{\nu}$ 3432 (br, crystal water), 3092 (m, CH_{ar}), 2922 (m, CH_{al}), 1729 (s, CO_{ester}), 1603 (s), 1583 (m), 1492 (m), 1454 (s), 1441 (s), 1372 (m), 1343 (s), 1280 (m), 1254 (s), 1126 (m), 1100 (m), 1023 (m), 841 (vs, PF), 768 (m), 752 (m), 560 (s) cm^{-1}. UV/vis (CH_3CN): λ_{abs} (ε) 517 (7500), 319 (28 800), 276 (34 700), 236 (29 900), 205 nm (31500 M^{-1} cm^{-1}). Emission (CH_3CN, 295 K, λ_{exc} = 517 nm): λ_{emiss} = 729 nm [τ = 722(5) ns]. Emission ($CH_3CH_2CH_2CN$, 77 K, λ_{exc} = 517 nm): λ_{emiss} = 707 nm [τ = 3309(15) ns]. Quantum yield (CH_3CN, λ_{exc} = 469 nm, 295 K): Φ = 0.003. CV (CH_3CN): $E_{1/2}$ = +0.81 (1e), −1.40 V (2e) vs Fc/Fc^+. Elem anal. Calcd for $C_{35}H_{32}F_{12}N_8O_2P_2Ru$ (987.68)·$5H_2O$: C, 39.00; H, 3.93; N, 10.40. Found: C, 39.03; H, 3.60; N, 10.40.

Acknowledgment. This work was supported by the Deutsche Forschungsgemeinschaft (Grant HE 2778/5-2). We thank Dr. F. Laquai and M. Meister (Max Planck Institute for Polymer Research, Mainz) for measuring the excited-state lifetime of **8**.

Supporting Information Available: X-ray crystallographic data for complex **8** in CIF format, X-ray structure of complex **8** (Figure S1), crystal and structure refinement data for complex **8** (Table S1), bond lengths and angles of complex **8** (Table S2), IR spectrum, UV/vis absorption and emission spectra, ^1H NMR spectrum, $^{13}C\{^1H\}$ NMR spectrum, HH COSY, NOESY, CH COSY, $^{13}C{-}^1H$ HMBC, and $^{15}N{-}^1H$ HMBC of **8** (Figures S2−S10), Cartesian coordinates of *cis-fac*-**9**, *trans-fac*-**9**, *mer*-**9**, the singlet ground state of **8**, the ^3MLCT state of **8**, graphical representation of the frontier orbitals of **8**, results of the TD-DFT (singlet) calculation of **8** (gas phase and CH_3CN), Cartesian coordinates of $Ni(CO)_3L$ complexes [L = κN(central pyridine)-ddpd, κN(terminal pyridine)-ddpd, NMe_3, NHC (1,3-dimethyl-2,3-dihydro-1*H*-imidazol-2-ylidene), PMe_3, PH_3, PF_3, pyridine, NH_3, CH_3CN, CH_3NC, correlation of A_1 stretching frequencies with C−O distances in $Ni(CO)_3L$ complexes. This material is available free of charge via the Internet at http://pubs.acs.org.

---

[33] Fallahpour, R.-A. *Synthesis* **2000**, *8*, 1138.

[34] Fallahpour, R.-A. *Eur. J. Inorg. Chem.* **1998**, 1205.

[35] Fallahpour, R.-A.; Neuburger, M.; Zehnder, M. *New J. Chem.* **1999**, *23*, 53.